

# Model Predictive Direct Torque Control for SPMSM with Load Angle Limitation

Mingdi Fan\*, Hui Lin, and Tianyi Lan

**Abstract**—The purpose of this paper is to describe a model predictive direct torque control (MPDTC) with load angle limitation for surface-mounted permanent magnet synchronous motor (SPMSM) drive system. In this paper, an exact discrete-time state-space model of SPMSM is presented, which improves the state prediction accuracy comparing to simple Euler approximation. A finite control set type MPDTC is used to select the optimum voltage vectors applying to the voltage source inverter (VSI). It makes full use of the inherent discrete nature of VSI, and according to the predefined cost function it chooses the optimal solution from the possible switching states. It has been found that with the proposed scheme SPMSM drives show adequate dynamic torque performance and considerable torque ripple reduction as compared to traditional direct torque control (t-DTC). With the load angle limitation in the cost function, the proposed scheme can prevent the PMSMs falling from synchronism.

## 1. INTRODUCTION

The permanent magnet synchronous motors (PMSMs) have been gaining popularity in high performance AC motor drives, owing to advances in manufacturing and commercializing PM materials, power electronics and digital signal processors, etc. Direct torque control (DTC), which is invented by Takahashi et al. [1] and Depenbrock [2] in the late 1980s, has revealed interesting performance in induction motor application where torque dynamic is essential [3, 4]. In view of the successful application of induction motors, it has been applied to the PMSMs [5–7]. Today, PMSMs with DTC are available on the market with several producers, different solutions and performance [8, 9].

In traditional DTC (t-DTC), when the torque is wanted to be increased, a voltage vector which increases the load angle (the angle between the stator flux linkage and the rotor flux linkage) is selected, and vice versa. However, with respect to the load angle, the torque of PMSMs has a maximum value. Taking the surface-mounted PMSM (SPMSM) as an example, when the load angle exceed  $90^\circ$ , the selected voltage vector which increases the load angle will decrease the torque. In order to prevent the PMSMs falling from synchronism, the load angle should be limited [10]. Pyrhonen [11] presented two approaches, for the limitation of the load angle in direct torque controlled electrically excited synchronous motor drives: indirect load angle control and direct load angle control. The indirect and direct approaches are combined by adding an adaptive term to the indirect torque limitation in PMSMs [12]. Zhang et al. [13] presented a direct load angle control scheme for Interior PMSM, which features low torque and flux ripples and almost fixed switching frequency by means of Space Vector Modulation (SVM). A novel DTC scheme was proposed for missile wing load emulation system running in special conditions, with torque increase by field-enhancing and keeping a constant load angle [14]. The aforementioned concepts are linear control combined with modulation schemes and nonlinear control based hysteresis bounds. With the fast development of digital signal processing techniques, new alternatives to both linear and nonlinear methods have been proposed using model predictive control (MPC) to achieve better performance [15–19].

---

*Received 11 February 2014, Accepted 26 February 2014, Scheduled 5 March 2014*

\* Corresponding author: Mingdi Fan (fanli1998@163.com).

The authors are with the School of Automation, Northwestern Polytechnical University, Xi'an, Shaanxi, P. R. China.

In recent decades, MPC, also referred to as receding horizon control, has been extremely successful in power electronics and motor drives applications [20, 21]. The main principle of MPC is to utilize a model of the systems in order to predict and optimize the future system behavior. In this paper, the finite control set type model predictive direct torque control (FCS-MPDTC) is suggested as an alternative to t-DTC for SPMSM. FCS-MPDTC makes full use of the inherent discrete nature of power inverters, and according to the minimization of the predefined cost function it chooses the optimal solution from the possible switching states [22]. In order to implement the FCS-MPDTC in a standard digital platform such as digital signal processor (DSP), a discrete time state space representation of Equation (5) should be obtained. The common approximation to obtain a discrete-time model for SPMSM is Euler method [23]. In fact the Euler approximation is a particular case of truncated Taylor series expansion, omitting the second-order and higher order terms [24]. Due to the omission, it may lead to poor accuracy for MPC [25–27]. In this paper, an exact discrete-time state-space SPMSM model is proposed which improves the state prediction accuracy, compared to simple Euler approximation. It is worth noting that the performance of MPC largely depends on the accuracy of the model. A more accurate model, performance can be better.

Another attractive feature of the presented control in this paper, with respect to other control, is the possibility to handle the nonlinearities and restrictions of the systems due to the existence of a cost function. The cost function, proposed in this paper, is divided into two main components: performance and restriction. The performance component ensures tracking of the reference torque and flux both in transient and steady state. The restriction region is the load angle limitation which prevents the PMSMs falling from synchronism. Some results to evaluate the performance of SPMSM drives were proposed in this paper. They are used to compare t-DTC and FCS-MPDTC in both steady-state and transient operating conditions. For the sake of comparison, these two control schemes are implemented in the same environment.

This paper is organized as follows: the discrete-time state-space motor model is analyzed in Section 2. In Section 3 the design of FCS-MPDTC for SPMSM is pointed out. The simulation and experimental results is shown in Section 4. Finally, concluding remarks are reported in Section 5.

## 2. SPMSM MODEL

The equations commonly used to model SPMSM (for SPMSM:  $d$ -axis stator inductance  $L_d$  is equal to  $q$ -axis stator inductance  $L_q$ , i.e.,  $L_d = L_q$ ) in the rotor reference frame ( $d$ - $q$ ) were derived as follows [28]:

$$\begin{cases} \frac{di_d}{dt} = \frac{1}{L_d} (u_d - R_s i_d + \omega_e L_q i_q) \\ \frac{di_q}{dt} = \frac{1}{L_q} (u_q - R_s i_q - \omega_e L_d i_d - \omega_e \psi_f) \end{cases} \quad (1)$$

$$\begin{cases} \psi_d = L_d i_d + \psi_f \\ \psi_q = L_q i_q \end{cases} \quad (2)$$

$$T_e = \frac{3}{2} p \psi_f i_q \quad (3)$$

$$\delta = \arctan \frac{\psi_q}{\psi_d} \quad (4)$$

where  $\omega_e$  is the electrical rotor angular speed and is related to the mechanical rotor angular speed  $\omega_m$ , i.e.,  $\omega_e = p\omega_m$ ,  $p$  is the pair of poles,  $u_d$  and  $u_q$  is the stator voltages in the  $d$ - $q$  frame,  $\psi_d$  and  $\psi_q$  is the stator fluxes in the  $d$ - $q$  frame, and  $i_d$  and  $i_q$  is the stator currents in the  $d$ - $q$  frame,  $R_s$  is the stator winding resistance,  $\psi_f$  is the permanent magnet rotor flux,  $T_e$  is the electromagnetic torque,  $\delta$  is the load angle.

It is possible to rewrite Equation (1) in continue-time state-space form:

$$\begin{cases} \dot{x} = Ax + Bu \\ y = Cx \end{cases} \quad (5)$$

where  $x = [i_d \ i_q]^T$ ,  $u = [u_d \ u_q \ \psi_f]^T$ ,  $y = [i_d \ i_q]^T$  and,

$$A = \begin{bmatrix} -\frac{R_s}{L_d} & \omega_e \frac{L_q}{L_d} \\ \omega_e \frac{L_d}{L_q} & -\frac{R_s}{L_q} \end{bmatrix} \quad B = \begin{bmatrix} \frac{1}{L_d} & 0 & 0 \\ 0 & \frac{1}{L_q} & \frac{-\omega_e}{L_q} \end{bmatrix} \quad C = \begin{bmatrix} 1 & 0 \\ 0 & 1 \end{bmatrix} \quad (6)$$

In Equation (6)  $R_s$ ,  $L_d$ ,  $L_q$  and  $\psi_f$  are the parameters of the SPMSM. The parameters variations can also have a negative impact on FCS-MPDTTC. Nevertheless, in this paper, in order to make the prediction problem can be computed in the range of microseconds on standard digital platforms, the parameters are assumed to be known and constant. Note that, the matrix  $A$  in Equation (5) includes the time-varying nature of the system (the electrical rotor angular speed  $\omega_e$ ) making a linear time variant (LTV) matrix, i.e.,  $A = A(\omega_e(t))$ . Compared with the sampling period, the mechanical time constant of the SPMSM is large enough, therefore, within each sampling period,  $\omega_e$  can be considered to be constant and equal to the measured value  $\omega_{e,k}$  at the sampling time  $kT_s$ , i.e.,  $\omega_e(t) = \omega_{e,k}, \forall t \in [kT_s, (k+1)T_s]$ . Then, the discrete-time state-space SPMSM model is derived as follow:

$$\begin{cases} x_{k+1} = A_k x_k + B_k u_k \\ y_k = C_k x_k \end{cases} \quad (7)$$

where  $A_k = e^{AT_s}$ ,  $B_k = \int_0^{T_s} e^{A\tau} B d\tau$  and  $C_k = C$ .

In order to obtain an accurate representation of  $A_k$ , as suggested by Miranda [29], the matrix  $A$  is separated into two matrices,  $A_c$  that does not depend on  $\omega_e$ , and  $A_\omega$  whose elements depend on  $\omega_e$ , and then  $A$  can be expressed as

$$A = A_c + A_\omega = \begin{bmatrix} -\frac{R_s}{L_d} & 0 \\ 0 & -\frac{R_s}{L_q} \end{bmatrix} + \begin{bmatrix} 0 & \omega_e \frac{L_q}{L_d} \\ -\omega_e \frac{L_d}{L_q} & 0 \end{bmatrix} \quad (8)$$

The discrete-time state-space model of induction motor proposed by Miranda [29] is not exact [24], which is evident from the following lemma.

*Lemma 1:* Let  $\Phi$ ,  $\Gamma \in R^{n \times n}$ . Then

$$e^{\Delta\Gamma} e^{\Delta\Phi} = e^{\Delta(\Gamma+\Phi)} \quad (9)$$

for all  $\Delta \in [0, \infty)$  if and only if  $\Gamma\Phi = \Phi\Gamma$ .

*Proof:* See [30].

However, in our case, for SPMSM ( $L_d = L_q = L_s$ ,  $L_s$  is the stator inductance),  $A_c = -\frac{R_s}{L_s}I$ , so  $A_c$  and  $A_\omega$  are commutative matrices, i.e.,

$$A_c A_\omega = A_\omega A_c = \omega_e \frac{R_s}{L_s} \begin{bmatrix} 0 & 1 \\ -1 & 0 \end{bmatrix} \quad (10)$$

Then, the matrix  $A_k$  can be derived as:

$$A_k = e^{AT_s} = e^{(A_c+A_\omega)T_s} = e^{A_c T_s} e^{A_\omega T_s} \quad (11)$$

where the matrix  $e^{A_c T_s}$  can be calculated offline since it is linear time invariant (LTI) matrixes. As explained earlier, matrix  $e^{A_\omega T_s}$  depends on  $\omega_e$  and is a LTV matrix. The instantaneous value of  $e^{A_\omega T_s}$  has to be updated at every sampling time. Considering the aforementioned assumption of  $\omega_e$ , i.e.,  $\omega_e(t) = \omega_{e,k}, \forall t \in [kT_s, (k+1)T_s]$ , an accurate representation of  $e^{A_\omega T_s}$  can be obtained using the Cayley-Hamilton theorem [31].

$$e^{A_\omega T_s} = \begin{bmatrix} \cos(\omega_e T_s) & \sin(\omega_e T_s) \\ -\sin(\omega_e T_s) & \cos(\omega_e T_s) \end{bmatrix} \quad (12)$$

Substitute Equation (12) into Equation (11), then

$$A_k = e^{A_c T_s} e^{A_\omega T_s} = e^{-\frac{R_s}{L_s} T_s} \begin{bmatrix} \cos(\omega_e T_s) & \sin(\omega_e T_s) \\ -\sin(\omega_e T_s) & \cos(\omega_e T_s) \end{bmatrix} \quad (13)$$

Then, the matrix  $B_k$  can be derived as:

$$B_k = \int_0^{T_s} e^{A\tau} B d\tau = A^{-1} (e^{AT_s} - I) B = A^{-1} (A_k - I) B \quad (14)$$

Finally, we will consider this discrete-time state-space model as an exact representation of SPMSM. The matrices  $A_k$ ,  $B_k$  and  $C_k$  will be used to predict the future behavior of the system.

### 3. PREDICTIVE CONTROL

FCS-MPDTC makes full use of the inherent discrete nature of the voltage source inverter (VSI), and predicts the future behavior in the next sampling period under each possible states of VSI by computation of the aforementioned discrete-time state-space model. The predictions are evaluated using the predefined cost function  $J$  and then the voltage vector that minimizes the cost function is selected and applied in the SPMSM. A block diagram of the proposed FCS-MPDTC scheme is shown in Figure 1.

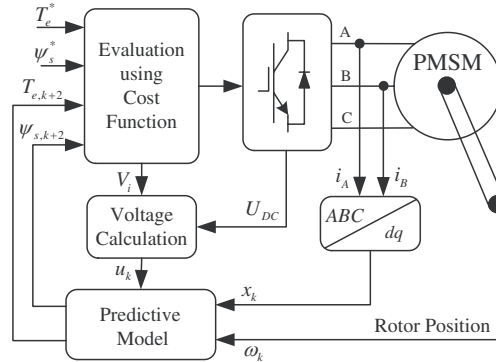


**Figure 1.** Block diagram of FCS-MPDTC.

As shown in Figure 1, the basic operation of the proposed control can be described as follows:

- Measurement:** The stator currents are measured by the current sensors; stator voltages are calculated using the magnitude of DC voltage and current switching state; and the electrical rotor angular speed can be obtained by an encoder or an observer.
- Prediction:** The measurements are used for prediction of electromagnetic torque, stator flux magnitude, load angle for all eight voltage vectors (a simple two-level VSI).
- Evaluation:** The predefined cost function is used to evaluate the predictions.
- Actuation:** The optimum voltage vectors, which are selected according to the evaluations, are applying to the VSI.

#### 3.1. Prediction with Delay Compensation

As compared with t-DTC, this kind of predictive control needs a high amount of calculations. Due to these calculations, the delay between the measurement and the actuation will cause errors if not considered. In this paper, this delay, which is the most important delay on the system, has been included in the design of the predictive process for the simulations, as well as for the experimental results. The graphically illustrations of the predictive process with and without delay compensation are shown respectively in Figure 2.

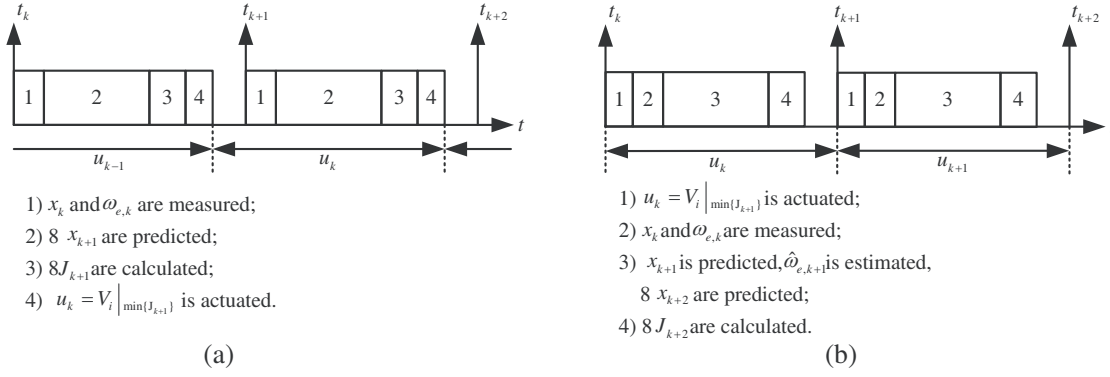


**Figure 2.** Graphically illustrations of the predictive process. (a) Without delay compensation. (b) With delay compensation.

As it can be observed in the Figure 2(a), the voltage vector  $u_k$  selected using measurement at sampling time  $t_k$  will be applied near  $t_{k+1}$ . As a consequence of this delay, the torque ripple and stator flux ripple will increase. The operation of the predictive process with delay compensation is shown in Figure 2(b). As discussed before, the time-varying term  $\omega_e$  is included in the predictive model and in the time interval  $kT_s$  ( $[t_k, t_{k+1}]$ ), it can be considered to be constant and equal to the measured value  $\omega_{e,k}$ . Note that, the predictive process with delay compensation needs  $\omega_{e,k+1}$  in the time interval  $kT_s$ . Using a second-order extrapolation obtained from the Lagrange interpolation formula [32], one-step-ahead estimation of  $\omega_e$  can be derived as:

$$\hat{\omega}_{e,k+1} = 3\omega_{e,k} - 3\omega_{e,k-1} + \omega_{e,k-2} \quad (15)$$

Then the instantaneous value of  $e^{A\omega T_s}$  in the time interval  $(k+1)T_s$  can be updated using  $\hat{\omega}_{e,k+1}$ . According to Equation (7),  $x_{k+2}$  can be predicted for each voltage vector. The voltage vector  $u_{k+1}$  that minimizes the cost function  $J_{k+2}$  is stored. At the beginning of the sampling time  $t_{k+1}$ ,  $u_{k+1}$  is applied to VSI. The estimation of  $\hat{\omega}_{e,k+1}$  and the prediction of  $x_{k+1}$  increase the calculation times but only marginally, as this calculation is performed only once.

### 3.2. Cost Function Design

In this paper, the cost function of FCS-MPDTC is divided into two main components: performance and restriction.

#### 3.2.1. Performance Component

In t-DTC, the reference stator flux magnitude is a constant, which is approximately equal to the permanent magnet rotor flux magnitude [33]. The main advantage of the constant stator flux magnitude (CSFM) control is that by limiting stator flux magnitude, the stator voltage requirement is kept comparably low [34]. And it gives a smooth control over the entire torque-speed region, with a seamless transition to field-weakening above the base speed.

In this paper, CSFM is used to implement the FCS-MPDTC, and the reference stator flux magnitude is equal to the permanent magnet rotor flux, i.e.,  $\psi_s^* = \psi_f$ . For the sake of clarity, the motor temperature effect on the permanent magnet is neglected, i.e., the rotor flux amplitude is a constant. Another input to FCS-MPDTC is the reference torque  $T_e^*$ , which is set either by the user or by a superimposed control (e.g., speed control).

The main criteria to evaluate the performance of FCS-MPDTC are torque and flux errors. The cost function to minimize the torque and flux errors is

$$J_P = \lambda_T \left( \frac{T_{e,k+2}^* - T_{e,k+2}}{T_{en}} \right)^2 + \lambda_\psi \left( \frac{\psi_s^* - \psi_{s,k+2}}{\psi_f} \right)^2 \quad (16)$$

where  $\lambda_T$  and  $\lambda_\psi$  are weighting coefficients.

### 3.2.2. Restriction Component

In traditional field oriented control (FOC) methods, the load angle can be controlled by adjusting the current references so that the maximum load angle is not exceeded [35]. When t-DTC is used, without the current loop, direct load angle adjustment is not possible [11]. As presented by Luukko et al. [10], indirect load angle limitation, which is implemented by modifying the reference torque, cannot be used in t-DTC. The reason is that reference torque limitation cannot ensure the stability if the load angle exceeds the maximum value. In that situation, the voltage vector which is selected from the switching table to accelerate the stator flux linkage vector increases the load angle and decreases the torque. This leads to a fast torque break down and loss of synchronism. T-DTC has no natural mechanism to prevent it. This problem occurs especially in the field-weakening application, where a large load angle is necessary to produce a high torque [11].

It is well known that, one of the major strengths of MPC is the ability to impose restrictions. In this paper, the load angle limitation is included simply in the cost function as follows:

$$J_R = \begin{cases} \lambda_\delta(\delta_{k+2} - \delta_{\max}) & \delta_{k+2} > \delta_{\max} \\ 0 & \delta_{k+2} \leq \delta_{\max} \end{cases} \quad (17)$$

where  $\lambda_\delta$  is weighting coefficients.

Finally, the cost function  $J$  of FCS-MPDTC is a combination of  $J_P$  and  $J_R$ , i.e.,  $J = J_P + J_R$ . However, there are three weighting coefficients, which are used to tune the importance of those control targets.

## 4. RESULTS

### 4.1. Simulation Results

In order to investigate the importance of load angle limitation under t-DTC or FCS-MPDTC, simulation models are constructed using Matlab/Simulink software package. Two control schemes are implemented in the same SPMSM drive using the same implementation conditions. The step size of simulation time is  $2 \mu\text{s}$ , and the sample time is  $100 \mu\text{s}$ . The SPMSM is  $Y$ -connected with parameters as in Table 1. The VSI used in simulation is IGBT inverter with  $+150$  to  $-150$  dc link voltage. The maximum switching frequency of the IGBT is set at  $10 \text{ kHz}$ .

**Table 1.** Parameters of SPMSM.

Rated DC voltage	$U_n$	300 (V)
Rated speed	$\omega_n$	3000 (r/min)
Rated torque	$T_{en}$	4.77 (Nm)
Number of pole pairs	$p$	5
Stator winding resistance	$R_s$	0.43 ( $\Omega$ )
Stator inductance	$L_s$	1.72 (mH)
Permanent magnet flux	$\psi_f$	0.05028 (Vs)
Moment of inertia	$M$	0.0006329 ( $\text{kgm}^2$ )
Friction constant	$B$	0.0003035 (Nms)

The simulation results of the two control schemes are shown in Figures 3. It is simulated with  $1500 \text{ r/min}$  ( $0.5\omega_n$ ) closed speed loop,  $4.77 \text{ Nm}$  load torque ( $T_L = T_{en}$ ), while the slope of the reference speed is limited to  $50000 \text{ r/min/s}$ . The speed loop proportional and integral parameters (in parallel PI form) are  $0.05$  and  $30$  respectively. In t-DTC, the band width of the torque hysteresis controller is  $0.1 \text{ Nm}$ , and the band width of the flux hysteresis controller is  $0.001 \text{ Vs}$ . And in FCS-MPDTC, the weighting coefficients  $\lambda_T$ ,  $\lambda_\psi$  and  $\lambda_\delta$  are  $1$ ,  $30$  and  $500$ , respectively.

It should be noted that, the reference torque, is limited to  $\pm 15 \text{ Nm}$ . And the maximum torque of the SPMSM under CSFM can be calculated as  $T_{e\_max} = 1.5p\psi_f^2/L_s = 11.0 \text{ Nm}$ . As discussed before, if the load angle is not limited, SPMSM will fall from synchronism. In Figure 3(a), the effectiveness of the

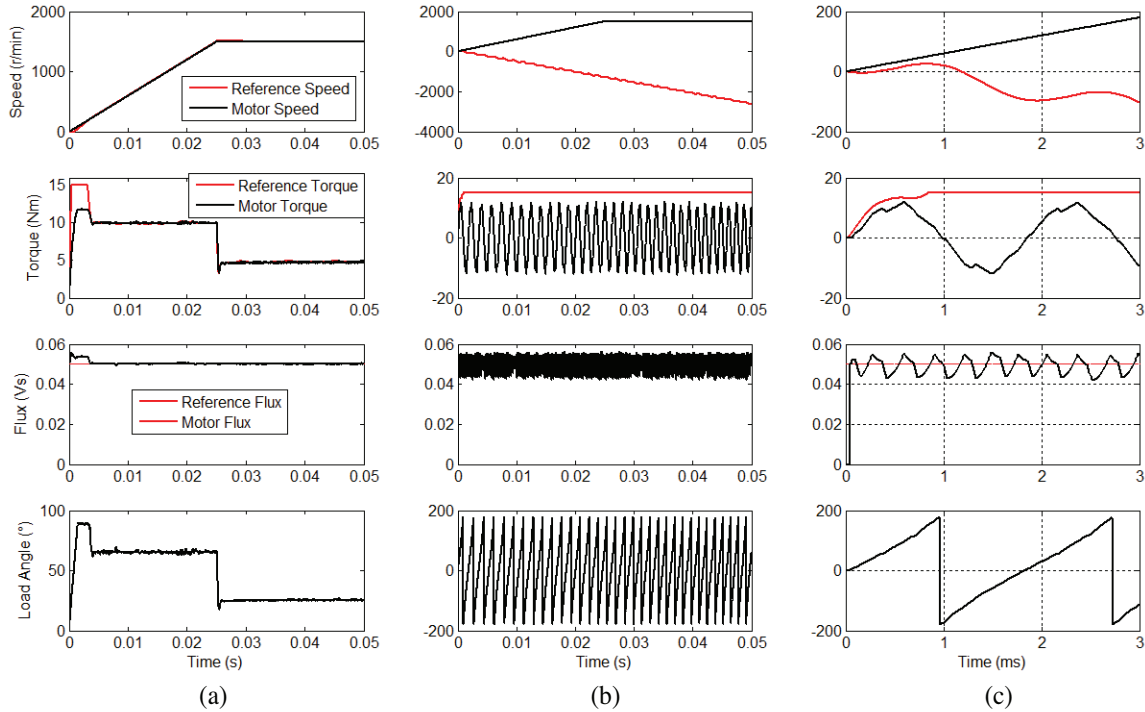


**Figure 3.** Simulation result of speed loop at  $0.5\omega_n$  with  $T_L = T_{en}$ . (a) FCS-MPDTC (0–0.05 s). (b) t-DTC (0–0.05 s). (c) t-DTC (0–3 ms).

load angle limitation in FCS-MPDTC is shown. Although a reference torque is greater than maximum torque, the SPMSM is still under control with FCS-MPDTC. However, t-DTC has no natural mechanism to prevent the motor falling from synchronism when the load angle exceeds  $90^\circ$ , as shown in Figures 3(b) and 3(c). In Figure 3(c), the simulation time is 3 ms that it is more clearly to investigate the process. The simulation results in Figure 3(c) are consistent with the aforementioned analysis in Section 3.2.

## 4.2. Experimental Results

These two control scheme are experimentally tested with a ten-pole 1.5 kW SPMSM. Detailed motor parameters are tabulated in Table 1. The sampling frequencies for these two control schemes both are 10 kHz. All these control algorithms and data logging are programmed in a DSP (TI: TMS320LF2812). The SPMSM is fed by a two-level VSI (MITSUBISHI: PM75RLA120). Hall-effect sensors (Xinmin: CSM025A and VSM025A) are used to measure the motor currents and DC voltage. The rotor mechanical position is measured by an incremental encoder (Bochen: BC66S).

### 4.2.1. Torque Dynamic Response

The torque dynamic response with t-DTC and proposed FCS-MPDTC are shown in Figures 4(a) and (b), respectively. The reference torque for both schemes is changed from  $-3$  to  $3$  Nm while the reference flux is kept as  $\psi_f$ . As shown in Figure 4, both torque direct control schemes have a fast dynamic response. This is the most important advantage against FOC. The striking feature is that there is less torque ripple when FCS-MPDTC is used. This superiority is due to the exact state-space model and the delay compensation.

### 4.2.2. Steady State Performance

The experimental results under steady state of SPMSM are shown in Figures 5–7. Figure 5 exhibits the load test results at speed of  $0.5\omega_n$ , where a 3 Nm load is applied to SPMSM. As shown in Figure 5, the ripples of speed, torque, flux and currents under t-DTC are all more than under FCS-MPDTC.

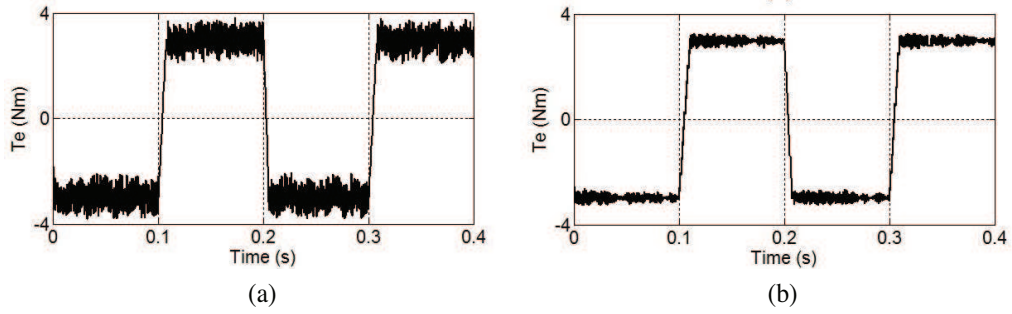


Figure 4. Torque dynamic response. (a) t-DTC. (b) FCS-MPDTC.

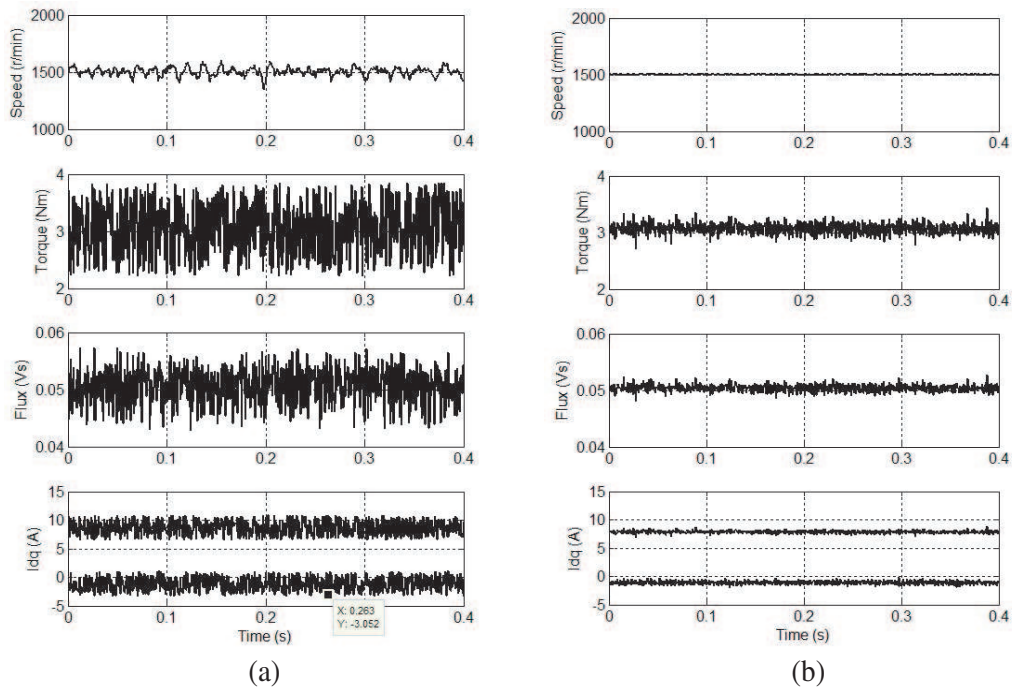


Figure 5. Steady state of SPMSM. (a) t-DTC. (b) FCS-MPDTC.

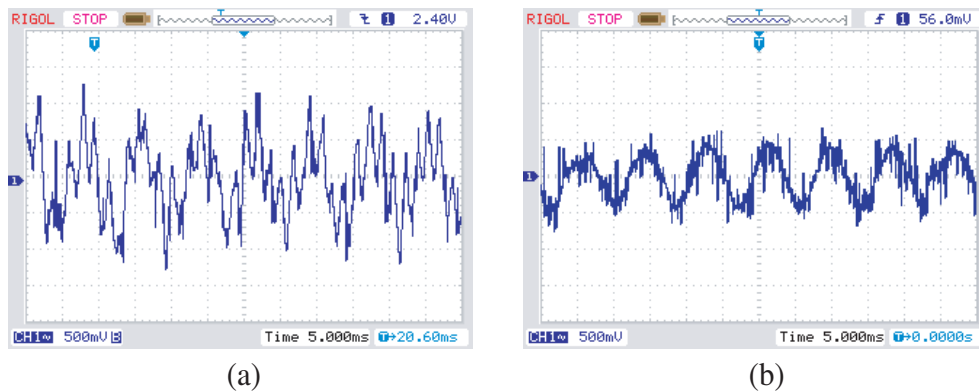
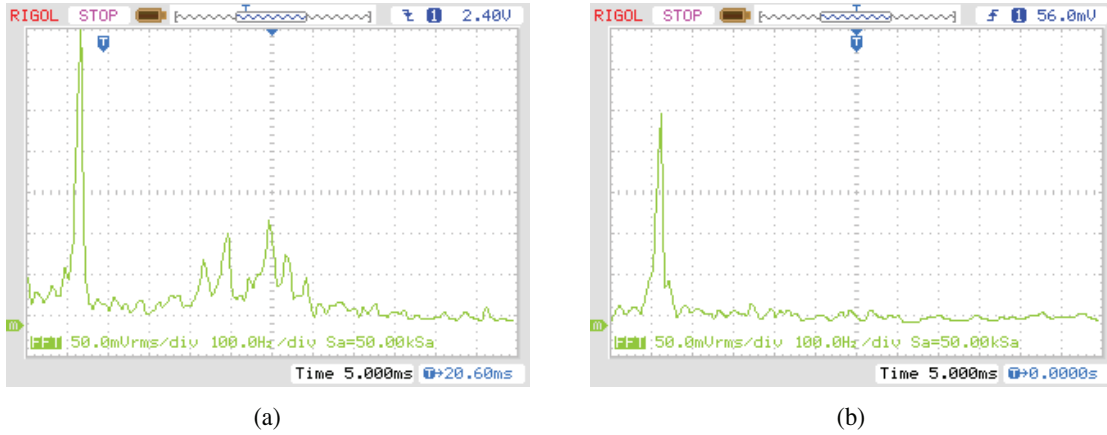
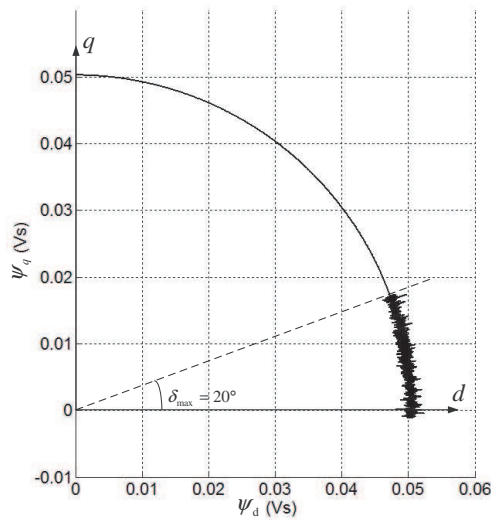


Figure 6. Experimental results of phase current (8 A/500 mV). (a) t-DTC. (b) FCS-MPDTC.



**Figure 7.** Frequency spectra of the phase current. (a) t-DTC. (b) FCS-MPDTC.



**Figure 8.** Load angle limitation with FCS-MPDTC ( $\delta_{\max} = 20^\circ$ ).

Figure 6 shows the phase current of SPMSM with t-DTC and FCS-MPDTC. It should be noted that the current ripple is significantly reduced when the proposed FCS-MPDTC is used. The frequency spectra for phase current are shown in Figure 7. The overall harmonic components stay at a relatively low level when the proposed FCS-MPDTC is used.

#### 4.2.3. Load Angle Limitation

The experiment of falling from synchronism has adverse effect on the SPMSM, like demagnetization. For verifying the effectiveness of load angle limitation and avoiding the adverse effect, a small  $\delta_{\max}$  is set at  $20^\circ$ . The reference torque for this experiment is changed from 0 to 4.77 Nm while the load torque is kept at 3 Nm. Figure 8 shows the load angle limitation results with FCS-MPDTC. Originally, the maximum load angle should be  $25.64^\circ$ , which can be calculated by the following equation:

$$\delta = \arcsin \left( \frac{4.77L_s}{1.5p\psi_f^2} \right) = 25.64^\circ \quad (18)$$

Nevertheless, as shown in Figure 8, the load angle is limited at  $20^\circ$  due to the cost function of FCS-MPDTC.

As shown in Figures 3–8, the proposed FCS-MPDTC improves the torque smoothness properties without deterioration of the torque dynamic performance of DTC. And as compared with t-DTC, it avoids the SPMSM falling from synchronism. It is noticed that with the proposed control the motor torque and flux is controlled to track its reference curve both at transient response and steady states.

## 5. CONCLUSIONS

To achieve the high-performance of SPMSM drive system, a finite control set type model predictive direct torque control (FCS-MPDTC) with load angle limitation was presented. The basic idea of FCS-MPDTC is to predict and optimize the future system behavior utilizing an exact discrete-time state-space model of the system. The results of the prediction are evaluated by the cost function and then the appropriate action is provided. The cost function, proposed in this paper, is divided into two main components: performance and restriction. The performance component ensures tracking of the reference torque and flux both in transient and steady state. The restriction region is the load angle limitation which prevents the PMSMs falling from synchronism. And in order to improve the performance, the time delay introduced by sampling and computation time is compensated during the predictive process.

The essential parameters of FCS-MPDTC are stator currents of two phases, voltage of the DC bus and the rotor position. As a result, the structure and the algorithm of FCS-MPDTC are simple and easy to implement. The simulation and experimental results of the proposed control scheme show that the SPMSM drive system has good performance during transient response and steady-state operations. It is a good alternative to t-DTC for SPMSM, and it can be applied to the servo systems.

## REFERENCES

1. Takahashi, I. and N. Noguchi, "A new quick response and high efficiency control strategy of an induction motor," *IEEE Transactions on Industrial Application*, Vol. 22, 820–827, 1986.
2. Depenbrock, M., "Direct self-control (DSC) of inverter-fed induction machine," *IEEE Transactions on Power Electronics*, Vol. 3, No. 4, 420–429, 1988.
3. Casadei, D., F. Profumo, G. Serra, et al., "FOC and DTC: Two variable schemes for induction motors torque control," *IEEE Transactions on Power Electronics*, Vol. 17, No. 5, 779–787, 2002.
4. Buja, G. S. and M. P. Kazmierkowski, "Direct torque control of PWM inverter-fed AC motors — A survey," *IEEE Transactions on Industrial Electronics*, Vol. 51, No. 4, 744–757, 2004.
5. Tang, L., L. Zhong, M. F. Rahman, and Y. Hu, "Novel direct torque controlled interior permanent magnet synchronous machine drive with low ripple in flux and torque and fixed switching frequency," *IEEE Transactions on Power Electronics*, Vol. 19, No. 2, 346–354, 2004.
6. Uddin, M. N., T. S. Radwan, G. H. George, and M. A. Rahman, "Performance of current controllers for VSI fed IPMSM drive," *IEEE Transactions on Industry Applications*, Vol. 36, No. 6, 1531–1538, 2000.
7. Adam, A. A. and K. Gulez, "A new sensorless hysteresis direct torque control algorithm for PMSM with minimum torque ripples," *COMPEL*, Vol. 28, No. 2, 437–453, 2009.
8. Kazmierkowski, P. M., L. G. Franquelo, J. Rodriguez, M. A. Perez, and J. I. Leon, "High-performance motor drives," *IEEE Industrial Electronics Magazine*, Vol. 5, No. 3, 6–26, 2011.
9. Wang, Y., J. G. Zhu, and Y. J. Guo, "A survey of direct torque control schemes for permanent magnet synchronous motor drives," *Proceedings of Power Engineering Conference 2007, (AUPEC 2007)*, 1–5, Australasian Universities, 2007.
10. Luukko, J., M. Niemela, and J. Pyrhonen, "Estimation of rotor and load angle of direct-torque-controlled permanent magnet synchronous machine drive," *IET Electric Power Applications*, Vol. 1, No. 3, 299–306, 2007.
11. Pyrhonen, O., "Analysis and control of excitation, field weakening and stability in direct torque controlled electrically excited synchronous motor drives," Department of Electrical Engineering, Lappeenranta University of Technology, Lappeenranta, Finland, 1998.

12. Luukko, J., O. Pyrhonen, M. Niemela, and J. Pyrhonen, "Limitation of the load angle in a direct-torque-controlled synchronous machine drive," *IEEE Transactions on Industrial Electronics*, Vol. 51, No. 4, 793–798, 2004.
13. Zhang, J., Z. Xu, L. Tang, and M. F. Rahman, "A novel direct load angle control for interior permanent magnet synchronous machine drives with space vector modulation," *Proceedings of Sixth International Conference on Power Electronics and Drive Systems, (PEDS 2005)*, Kuala Lumpur, Malaysia, 2005.
14. Li, B. and H. Lin, "Torque increase by field enhancing with constant load-angle control for SPMSM," *Dianji yu Kongzhi Xuebao/Electric Machines and Control*, Vol. 14, No. 5, 56-60+67, 2010.
15. Pacas, M. and J. Weber, "Predictive direct torque control for the PM synchronous machine," *IEEE Transactions on Industrial Electronics*, Vol. 52, No. 5, 1350–1356, 2005.
16. Geyer, T., G. Papafotiou, and M. Morari, "Model predictive direct torque control part I: Concept, algorithm, and analysis," *IEEE Transactions on Industrial Electronics*, Vol. 56, No. 6, 1894–1905, 2009.
17. Lee, J. H., "Model predictive control: Review of the three decades of development," *International Journal of Control Automation and Systems*, Vol. 9, No. 3, 415–424, 2011.
18. Cortes, P., J. Rodriguez, C. Silva, and A. Flores, "Delay compensation in model predictive current control of a three-phase inverter," *IEEE Transactions on Industrial Electronics*, Vol. 59, No. 2, 1323–1325, 2012.
19. Preindl, M. and S. Bolognani, "Model predictive direct torque control with finite control set for PMSM drive systems, Part 1: Maximum torque per ampere operation," *IEEE Transactions on Industrial Informatics*, Vol. 9, No. 4, 1912–1921, 2013.
20. Cortes, P., M. P. Kazmierkowski, R. M. Kennel, D. E. Quevedo, and J. Rodriguez, "Predictive control in power electronics and drives," *IEEE Transactions on Industrial Electronics*, Vol. 55, No. 12, 4312–4324, 2008.
21. Drobnic, K., M. Nemeč, D. Nedeljkovic, and V. Ambrozic, "Predictive direct control applied to AC drives and active power filter," *IEEE Transactions on Industrial Electronics*, Vol. 56, No. 6, 1884–1893, 2009.
22. Xia, C., Y. Wang, and T. Shi, "Implementation of finite-state model predictive control for commutation torque ripple minimization of permanent-magnet brushless DC motor," *IEEE Transactions on Industrial Electronics*, Vol. 60, No. 3, 896–905, 2013.
23. Mariethoz, S., A. Domahidi, and M. Morari, "High-bandwidth explicit model predictive control of electrical drives," *IEEE Transactions on Industry Applications*, Vol. 48, No. 6, 1980–1992, 2012.
24. Rojas, C. A., J. I. Yuz, C. A. Silva, and J. Rodriguez, "Comments on 'Predictive torque control of induction machines based on state-space models'," *IEEE Transactions on Industrial Electronics*, Vol. 61, No. 3, 1635–1638, 2014.
25. Linder, A., R. Kanchan, R. Kennel, and P. Stolze, *Model-based Predictive Control of Electric Drives*, Cuvillier Verlag Gottingen, Munich, Germany, 2010.
26. Joshi, B. and M. Chandorkar, "Time discretization issues in induction machine model solving for real-time applications," *IEEE IEMDC 2011*, 675–680, 2011.
27. Diao L., D.-N. Sun, K. Dong, L.-T. Zhao, and Z.-G. Liu, "Optimized design of discrete traction induction motor model at low-switching frequency," *IEEE Transactions on Power Electronics*, Vol. 28, No. 10, 4803–4810, 2013.
28. Pillay, P. and R. Krishnan, "Modeling, simulation, and analysis of permanent-magnet motor drives. I. The permanent-magnet synchronous motor drive," *IEEE Transactions on Industry Applications*, Vol. 25, No. 2, 265–273, 1989.
29. Miranda, H., P. Cortes, J. I. Yuz, and, J. Rodriguez, "Predictive torque control of induction machines based on state-space models," *IEEE Transactions on Industrial Electronics*, Vol. 56, No. 6, 1916–1924, 2009.

30. Bernstein, D. S., *Matrix Mathematics: Theory, Facts, and Formulas with Application to Linear Systems Theory*, Princeton Univ. Pres, Princeton, NJ, USA, 2009.
31. Visser, M., S. Stramigioli, and C. Heemskerk, "Cayley-Hamilton for roboticists," *Proceedings of the 2006 International Conference on Intelligent Robots and Systems (IEEE/RSJ 2006)*, 4187–4192, Beijing, China, 2006.
32. Rodriguez, J., J. Pontt, C. A. Silva, P. Correa, P. Lezana, P. Cortes, and U. Ammann, "Predictive current control of a voltage source inverter," *IEEE Transactions on Industrial Electronics*, Vol. 54, No. 1, 495–503, 2007.
33. Ozturk, S. B., "Direct torque control of permanent magnet synchronous motors with non-sinusoidal back-EMF," Ph.D. Texas A & M University, Texas, United States, 2008.
34. Krishnan, R., *Permanent Magnet Synchronous and Brushless DC Motor Drives*, Taylor & Francis Group, 2010.
35. Mard, M., J. Niiranen, and V. Vauhkonen, "The control properties of synchronous motors within load angles of 90 degrees," *Proceedings of the International Conference on Electrical Machines (ICEM90)*, 434–439, 1990.